MICRO-TETHERING FOR IN-PROCESS STICTION MITIGATION OF HIGHLY COMPLIANT STRUCTURES

Ian B. Flader, Yunhan Chen, Dongsuk D. Shin, David B. Heinz, Lizmarie Comenencia Ortiz, Anne L. Alter, Woosung Park, Kenneth E. Goodson, and Thomas W. Kenny
Stanford University, Stanford, CA, USA

ABSTRACT

This work demonstrates, for the first time, a post-fabrication technique for creating highly compliant structures inside a hermetic, wafer-scale encapsulation process. By tethering large, free-moving structures during fabrication this method mitigates in-process stiction by selectively detaching devices post-fabrication. The tethers in this work were attached to differential resonant beam accelerometers (DRBA), and were designed for detachment by two methods: Joule heating and shear stressing. Our results show that the device can be successfully detached by both methods, indicated by the device sensitivity increase from ~100 Hz/g to ~400 Hz/g.

INTRODUCTION

Stiction in MEMS is a paramount issue that has received much attention since the field's inception [1]. Researchers have found ways to add coatings and other surface augmentations to circumvent in-process stiction. Unfortunately, many of these methods have strict thermal budgets or involve contamination that is not compatible with downstream fabrication processes. The devices in this study were fabricated in a unified Stanford Epi-seal process [2] where low thermal budget and contaminated materials cannot be incorporated.

Compliant structures are more likely to experience stiction due to larger static displacements as compared to stiffer devices for the same applied force. Additionally, the devices are encapsulated under low pressures [3], which reduces the damping inside the cavity. This near vacuum enables high quality factors, but also provides little resistance to large deflections of compliant devices at their resonant frequencies. This leads to surface contacts and stiction of released structures during fabrication.

Stiction tends to occur during releasing phases of MEMS fabrication. This is typically a result of wet hydrofluoric acid etching of sacrificial silicon dioxide, due to capillary and adhesion forces, in addition to the relatively high surface area to volume ratios encountered in MEMS devices. The Stanford encapsulation process utilizes an anhydrous vapor hydrofluoric (HF) acid system to circumvent potential stiction issues during the releasing step. This system also utilizes ethanol and a reduced pressure to mitigate the stiction effect. However, the reaction products of the sacrificial material, SiO_2, and HF include water regardless of the phase of the etchant. Ideally, the reduced pressure prevents the formation of aqueous byproducts. However, stiction may still occur if the temperature and pressure are not properly regulated.

Further, in-process stiction becomes more problematic when the process involves high temperature steps. After releasing, the perforations allowing vapor HF to etch the sacrificial material are sealed using an epitaxial reactor. This process undergoes an 1100C annealing step. Any devices which may be stuck at this point will become permanently welded to the surface which they are contacting. Further, the released devices undergo another high temperature (800C) step during the isolation deposition, making it crucial to prevent stiction before these high temperature steps take place.

Many studies have investigated the stiction properties of the Stanford encapsulation process [4,5]. These works show the inverse relation between the spring stiffness of a structure and the survival rate of devices fabricated in the Epi-seal process. High yield has been demonstrated for this process for structures with spring stiffness >20 N/m. However, this provides a significant challenge for fabricating devices whose performance directly relates to the size or compliance of the incorporated structure. Compliant devices require less stiction and adhesion forces to bring surfaces into contact, and to maintain that contact. Unfortunately, many devices directly benefit from large released areas. Therefore, there is a tradeoff between device performance and yield.

To overcome this, silicon tethers are proposed with the intention of post-fabrication augmentation. Previous works have created stress concentrating features that are intended locations of fracture post-fabrication [6]. Others have used the principle of Joule heating to heat the tether until the point of melting and device separation [7]. In this work, we attempt to bypass the performance-yield tradeoff in the differential resonant beam accelerometer (DRBA) by tethering the large proof mass. This device directly benefits from higher compliance, as the acceleration sensitivity of the device is increased by making the proof mass larger. To prevent in-process stiction of this highly compliant structure, the device was fabricated with a tether to hold the proof mass in place. After successful fabrication, the tether was designed to detach by Joule melting or shear breaking.

DESIGN AND EXPERIMENTAL SETUP

The devices studied in this work were differential resonant beam accelerometers (DRBA), similar to work presented in [8]. DRBAs were fabricated in <111> single crystal silicon with a 40μm thick device layer utilizing a unified, etch-hole free Stanford encapsulation process. This process allows for the use of large (>50μm) and small (>0.7μm) transduction gaps [2]. The differential resonant beam accelerometer operates under the frequency-strain

relationship. Two resonator beams are connected to a large, free-moving proof mass. Under acceleration, the proof mass pivots relative to its single anchor point. Since each beam is connected to the proof mass and located on either side of the pivot point, one resonant beam will become under tension while the other beam will become under compression. The beam under tension will experience an increase in frequency, while the beam under compression will experience a decrease in frequency. This differential frequency signal is then used to determine the acceleration applied to the device.

A tethering system was developed to secure the highly compliant proof mass of the DRBA during the fabrication process. Figure 1 shows the geometry of the resonant accelerometer which incorporates two resonant beams, a large proof mass, and a tether connecting the proof mass to a second anchor. High acceleration and releasing stages of device fabrication are prone to in-process stiction of large devices. Therefore, the tether was designed to hold the proof mass in place during fabrication to avoid stiction, and broken by Joule heating or shearing later when the device was fully fabricated inside the wafer encapsulation. The proof mass used in this study was approximately 1mm by 1mm in size, while the tether was designed to be 100µm by 2µm. The resonant beams were designed with dimensions of 159µm by 3µm. Figure 1 also shows that a silicon heater was incorporated in the design of the differential resonant beam accelerometer. The out-of-plane heater was fabricated by etching DRIE trenches inside the silicon encapsulation layer. The trenches were refilled with silicon nitride to act as an electrical and thermal insulator. While the heater was not actively utilized in this work, it does heat passively during the Joule heating process.

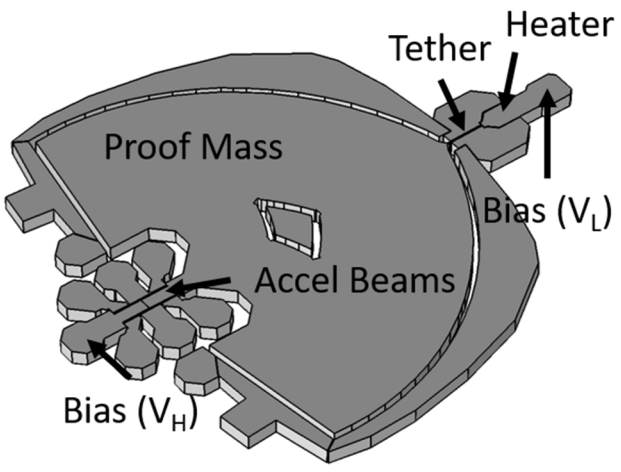

Figure 1: Device schematic for the tethered differential resonant beam accelerometer. The released DRBA is doubly anchored at the two voltage terminals, V_H and V_L. Joule heating is achieved by applying a potential voltage difference across the high and low voltage terminals. Out-of-plane heater contact also shown.

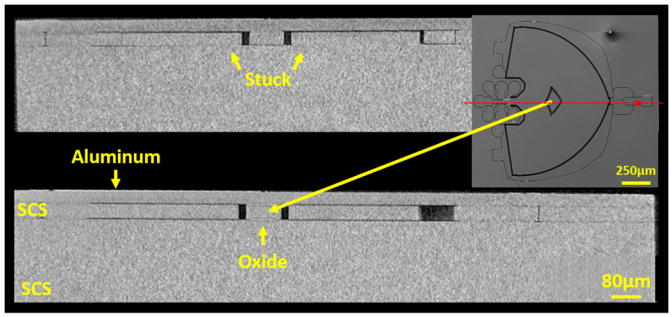

Figure 2: X-ray computed tomography image of two differential resonant beam accelerometers. Top: Device stuck to substrate. Bottom: Device free from stiction.

A ZEISS Xradia 520 Versa X-ray CT was used to create x-ray computed tomography (XCT) cross-sectional images of fabricated devices, shown in Figure 2. The fabricated wafers were cut into 2mm by 2mm dies and cross-sectional images of two devices were taken near the pivot axis of each device. Figure 2 (top) shows the large accelerometer proof mass stuck to the substrate floor of the wafer encapsulation after fabrication. Figure 2 (bottom), shows that in-process stiction of the proof mass may be avoided by incorporating tethered techniques during fabrication. The designed footprint of each device in Figure 2 were identical, signifying that in-process stiction provides a significant challenge to compliant device fabrication.

RESULTS AND DISCUSSION

The fabricated wafers were diced into 2mm by 2mm dies and wirebonded to create electrical contact to the accelerometer resonant beam drive and sense electrodes, device electrical vias, and tether electrical vias. The device and tether contacts were used as high and low voltage terminals, respectively. A current was passed through the device by applying a high voltage to the device bias, while maintaining the tether bias at ground, as shown in Figure 1. No voltage was applied to the encapsulation heater. Joule heating was achieved in this way until the tether reached a high enough temperature to melt. Figure 3 shows infrared imaging for various amounts of current passing through a device of ~250Ω resistance between the device and tether contact. First (Figure 3 (a)), no voltage was applied to the device to obtain a baseline image. Then (Figure 3 (b)), 5.71V was applied at the device bias. Small amounts of infrared radiation can be observed at this point. The bias voltage was then increased to 8.71V in Figure 3 (c). As can be seen, more heating occurs which results in more infrared radiation. Finally, the bias voltage was increased to 9.71V in Figure 3 (d). The measured current increased to 70mA and heating of the tether region, as well as a nitride-isolated region inside the encapsulation layer, became very visible. After maintaining the bias and current at the levels in Figure 3 (d) the device detached and there was no longer current flow from the high voltage terminal to the low voltage terminal.

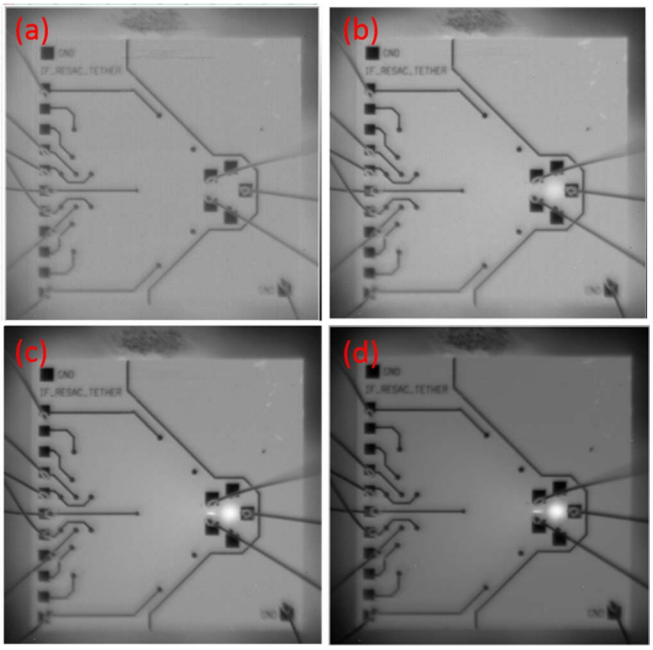

Figure 3: Infrared images of tethered device as heating is applied. Heating was concentrated in the tethered beam and nitride encapsulation isolation. (a) No heat applied, (b) 5.71V at 23mA, (c) 8.71V at 34mA, (d) 9.71V at 70mA. Device separation occurred shortly after 70mA. Measured resistance was ~250Ω.

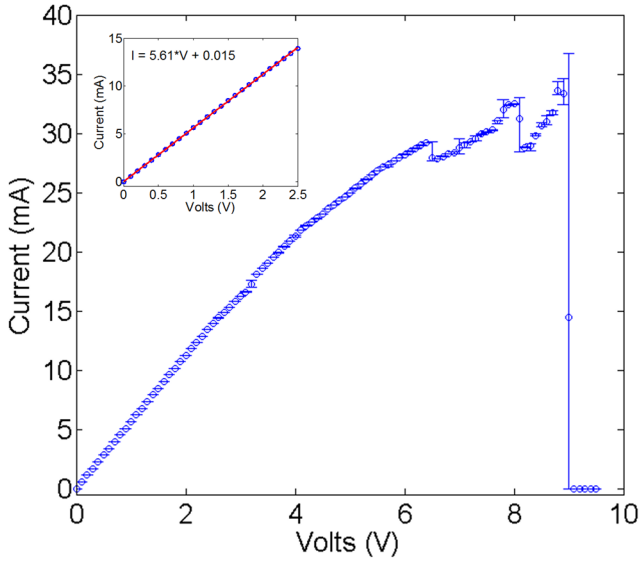

Figure 4: Joule breaking of the tether. Detachment occurred at 9V with <40mA current. Initial measured resistance was ~178Ω. Inset: ohmic region of the tether up to 2.5V and less than 14mA.

This test was repeated for another device with a resistance of ~178Ω. Figure 4 shows the current relationship to applied voltages across the device. Again, the device contact was used as a high voltage terminal while the tether contact was maintained at ground. The voltage was swept up from 0V to 9.5V in 0.1V increments while the current was measured at each interval. Current measurements were made 10 times with 1 second intervals (not including measurement time). The mean value of each measurement has been plotted in Figure 4 with error bars representing the spread of the measurements. As shown in Figure 4, the device leaves the linear ohmic region at around 2.5V and ~14mA. As the device heats more, the current-voltage relationship becomes more nonlinear until the inevitable failure of the tether. The tether became unstable when 9V was applied and ultimately failed. No current could flow for subsequent measurements indicating that the tether had indeed failed, as anticipated.

Acceleration sensing is shown in Figure 5 to demonstrate the functioning DRBA. A 10V bias was applied to the device and the accelerometer beams were excited with a $10mV_{ac}$ signal from a Zurich Instrument HF2LI system. Figure 5 (left) shows the open-loop frequency response of one accelerometer beam before separation of the proof mass. The device was operated in a tilt test and the resonant frequency of the beam was monitored. When the DRBA undergoes a -1g acceleration the resonator beam is under tension, and the resonant frequency increases. Likewise, when the device undergoes a +1g acceleration the beam's resonant frequency decreases. In Figure 5 (right), we show the tilt test results for the same device after detachment. While the proof mass is attached, the accelerometer is much less sensitive (~140.3 Hz/g) to acceleration, as expected. The device operates under much higher acceleration sensitivity once the tether is removed either by Joule or shear breaking (~462.9 Hz/g).

Another method for detaching the proof mass employed a large shearing stress across the tether to induce fracture. The tether was notched as shown in Figure 6 to act as a stress concentrator. Pinning protrusions were incorporated in the design to concentrate stress inside the notch during deflection of the proof mass. The free-moving proof mass breaks free when a critical displacement has been reached, yielding notch stresses in excess of the fracture limit of silicon (~1-20 GPa). This method was achieved using an impact mechanism where the device undergoes a rigid impact with a fixed frame. The device was successfully separated when subjected to a 10,200g impact. The reference acceleration was monitored using a PCB Piezotronics 350D02. The large gaps afforded by this unique fabrication process prevented potential over travel and contact between the proof mass and surrounding electrodes. A 15µm wide gap was used for the proof mass of these devices.

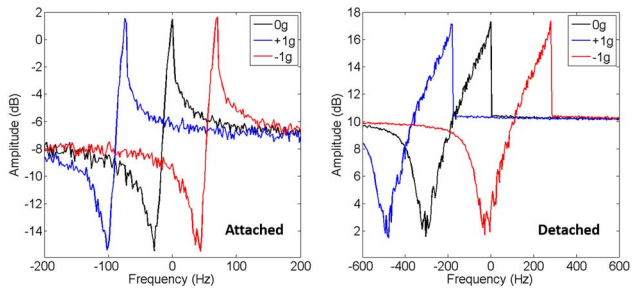

Figure 5: Frequency response before and after detachment.

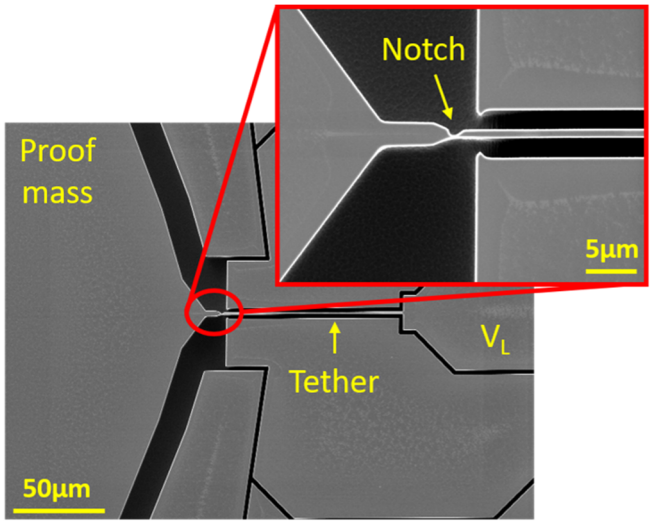

Figure 6: SEM of tether beam design. Inset: close-up of notched design for shear breaking.

Additionally, some tethered DRBAs were observed to be functional without any post-fabrication conditioning. The proof mass of these devices had become separated during the fabrication process, after the critical in-process stiction steps. Table 1 provides a summary of the DRBA results presented in this work. Results for resonant frequency of each beam, frequency split, and sensitivity are presented for each of the detachment methods: Joule breaking, shear breaking, and fabrication breaking. Each method produced similar results.

Table 1. Tethered Accelerometer Summary of Results

	Joule Break		Shock Break		Fab Break	
	Attached	Detached	Attached	Detached	Attached	Detached
$f_{b,1}$ (kHz)	785.563	798.046	793.461	796.206	-	824.132
$f_{b,2}$ (kHz)	800.819	804.130	803.879	811.877	-	835.818
Δf (kHz)	15.256	6.084	10.418	15.671	-	11.686
SF (Hz/g)	140.3	462.9	256.5	460.9	-	408.8

CONCLUSION

Differential resonant beam accelerometers were fabricated using a unified Stanford encapsulation process. This etch-hole free, large gap process allows for the fabrication of very large, compliant structures. The large DRBA proof mass was securely tethered during processing to circumvent the in-process stiction that very compliant structures face. Devices were successfully fabricated and two methods for detaching the proof mass for high-sensitivity operation were shown: Joule and shear detachment. Additionally, some device tethers were fragile enough to break during fabrication. However, this fracture occurred after the critical stiction point that plagued untethered devices, and operational DRBAs were obtained without additional conditioning. Tethered DRBAs were measured to have a sensitivity of ~100 Hz/g. Devices that were untethered by any of the described methods resulted in sensitivities of ~400 Hz/g.

ACKNOWLEDGEMENTS

This work was supported by the Defense Advanced Research Projects Agency Precise Robust Inertial Guidance for Munitions (PRIGM) Program, managed by Dr. Robert Lutwak. The fabrication was performed at the Stanford Nanofabrication Facility and the Laurie Nanofabrication Facility at the University of Michigan.

REFERENCES

[1] R. Maboudian and R. T. Howe, "Critical review: Adhesion in surface micromechanical structures," *J. Vac. Sci. Technol. B*, vol. 15, no. 1, pp. 1–20, 1997.

[2] Y. Yang, E. J. Ng, Y. Chen, I. B. Flader, and T. W. Kenny, "A Unified Epi-Seal Process for Fabrication of High-Stability Microelectromechanical Devices," Journal of Microelectromechanical Systems, Vol. 25, No. 3, pp. 489-497, Jun 2016.

[3] V.A. Hong, J. Stehle, C.H. Ahn, D.B. Heinz, G. Yama, B. Kim, G.J. O'Brien, and T.W. Kenny, "Capacitive sensor fusion: Co-fabricated X/Y and Z-axis accelerometers, pressure sensor, thermometer," 2015 Transducers - Solid-State Sensors, Actuators and Microsystems, pp. 295-298, Jun 2015.

[4] D. B. Heinz, V. A. Hong, C. H. Ahn, E. J. Ng, Y. Yang, and T. W. Kenny, "Experimental Investigation Into Stiction Forces and Dynamic Mechanical Anti-Stiction Solutions in Ultra-Clean Encapsulated MEMS Devices," Journal of Microelectromechanical Systems, Vol. 25, No. 3, pp. 469-478, Jun 2016.

[5] D. B. Heinz, V. A. Hong, E. J. Ng, C.H. Ahn, Y. Yang, and T. W. Kenny, "Characterization of stiction forces in ultra-clean encapsulated MEMS devices," MicroElectroMechanicalSys., pp. 588-591, Jan 2014.

[6] D. Hériba, J. Agnus, V. Petrini, and M. Gauthier, "A mechanical de-tethering technique for silicon MEMS etched with a DRIE process," Journal of Micromech. and Microeng., Vol. 19, No. 5, April 2009.

[7] Y. Chiu, K. Chang, R. W Johnstone and M. Parameswaran, "Fuse-tethers in MEMS," J. of Micromech. and Microeng., Vol. 16, Jam 2006.

[8] D. L. Christensen, C. H. Ahn, V. A. Hong, E. J. Ng, Y. Yang, B. J. Lee, and T. W. Kenny, "Hermetically encapsulated differential resonant accelerometer," 2013 Transducers & Eurosensors: Solid-State Sensors, Act. and Microsys.,pp. 606-609, Jun 2013.

CONTACT

*I. B. Flader, tel: +1-469-371-5384; iflader@stanford.edu